ORIGINAL ARTICLE

Synthesis of Hg metal complex and its application to reduce the optical band gap of polymer

Karzan A. Abdalkarim [a]**, Shujahadeen B. Aziz** [b,c,*]**, Rebar T. Abdulwahid** [b,d]**,
Saad M. Alshehri** [e]**, Tansir Ahamad** [e]**, Jihad M. Hadi** [f]**, Sarkawt A. Hussein** [b]

[a] *Department of Chemistry, College of Science, University of Sulaimani, Qlyasan Street, Sulaimani 46001, Kurdistan
Regional Government, Iraq*
[b] *Hameed Majid Advanced Polymeric Materials Research Lab., Physics Department, College of Science, University of
Sulaimani, Qlyasan Street, Sulaimani 46001, Kurdistan Regional Government, Iraq*
[c] *Department of Civil Engineering, College of Engineering, Komar University of Science and Technology, Sulaimani 46001,
Kurdistan Regional Government, Iraq*
[d] *Department of Physics, College of Education, University of Sulaimani, Old Campus, Sulaimani 46001, Kurdistan
Regional Government, Iraq*
[e] *Department of Chemistry, King Saud University, P.O. Box 2455, Riyadh 11451, Saudi Arabia*
[f] *Department of Medical Laboratory of Science, College of Health Sciences, University of Human Development, Kurdistan
Regional Government, Iraq*

Abstract This study explored a new approach to fabricate the Schiff base ligand system from both ethylenediamine and 3-chloro-2-butanone. Through coordination chemistry, the mercury Hg (II) complex was achieved from the ligand and then embedded in the polyvinyl alcohol (PVA) host using a solution casting technique to prepare polymer composites (PCs). Both UV–visible and Fourier-transform infrared (FTIR) spectroscopies highlighted the formation of the Hg (II) metal complex. These techniques confirmed the synthesis of the Hg (II) metal complex. The X-ray diffraction (XRD) pattern of the polymer composite has shown a significant enhancement in its amorphous nature compared to the pure PVA host. The thermal analysis spectra for the Hg (II) complex revealed high thermal stability. The occurrence of the complexation between the Hg (II) and host matrix of the PVA was identified from the wide shifting of UV–vis absorption and peak

---

* Corresponding author at: Hameed Majid Advanced Polymeric Materials Research Lab., Physics Department, College of Science, University of Sulaimani, Qlyasan Street, Sulaimani 46001, Kurdistan Regional Government, Iraq.

E-mail address: shujahadeenaziz@gmail.com (S.B. Aziz).

shifting with intensity reduction of the FTIR spectra. Tauc's method has been employed to evaluate the optical band gap, and determine the types of electronic transitions. The results have shown that the samples were exhibiting an indirect forbidden electron transition, with a significant reduction in the optical band gap of a doped sample that approaching inorganic semiconductor based-materials. In addition, the optical study has exposed the role of the Hg (II) complex in tuning the refractive index of the host polymer. Ultimately, the absorption edge was found to be shifted to the lower photon energy upon the insertion of the Hg (II) complex. The PVA doped sample displayed a substantial shift in band gap from **6.2 eV to 1.2 eV**.

1. Introduction

Metal complexes for Schiff bases ligands have a broad range of applications in many fields like medicine, industrial, biological, chemistry, and so on. It can be easily synthesized to form stable coordination complexes with almost all metal ions. Recently, many studies have been done on biological activities of the Schiff base ligands counting antifungal, anticancer, antibacterial, antioxidant, anti-inflammatory, antimalarial, as well as antiviral activity. As a subsequent, it can act as a catalyst in many reactions, including reactions of polymerization, oxidation of organic compounds, thionyl chloride reduction, etc. (Hazari et al., 2012; Shi et al., 2020; Xu et al., 2020; Wang et al., 2020; Mahmoudi et al., 2020; Abu-Dief and Mohamed, 2015). It is well-identified that metals are of economic value for industrial purposes; however, they have a drawback of contributing to the utmost environmental pollution (Brza et al., 2019). On the other hand, a water-soluble complex catalyst is being extensively studied, combine the benefits of heterogenous and homogenous catalysis. The required catalysis can be produced for several reactions from its vast number of available water-soluble ligands (Herrmann and Kohlpaintner, 1993). Metal-transition complexes may have unique electronic and optical properties as a high-interest class of optoelectronic materials, resulting from their rich ligands and metal centres electronic structures. Polymers comprising metal complexes show outstanding electronic and optical properties that vary from original polymers with a pure organic skeleton (Liu et al., 2012). In particular, the interest in narrowing the band gap of these materials has grown in the last few years, and worldwide research findings have shown practical applications opportunities in the field of infrared optoelectronics and solar cells (Kershaw et al., 2013).

Thus, metal complexes can play the key role in a variety of applications, for instance, conversion of solar energy, polymeric light-emitting diodes, photo-refraction, chemical sensors, electrochromic as well as electrocatalysis (Liu et al., 2002). Mercury (II) compounds are used in numerous expanses including polymers, cosmetics, paper, dyes, fluorescent lamps, and to a lesser extend in batteries. Divalent mercury ion possesses ten electrons filled its 5d energy level, thus it has a strong potential to form complex quickly. Therefore, a metal complex comprising Hg (II) demonstrated different structural configurations, in which various coordination numbers were presented by a metal ion (Morsali and Masoomi, 2009). The literature has shown the importance of the dithiocarbonate derivative for numerous purposes due to its excessive favour to form a complex with metal ions, which is found crucial for solving many problems (Islam et al., 2016; Zhang et al., 2008; Menezes et al., 2005).

Previous work confirmed that strong interaction between the fillers and the host polymers leads to an increase in absorption and reduction in optical band gap (Aziz et al., 2016). This is correlated to the providing many trapping sites in polymer bodies as charge carriers. Based on these facts, accurate measurement of optical properties is of essential importance in terms of fundamental and industrial point views.

Polyvinyl alcohol (PVA) is known as a low-cost, easily degradable and water-soluble crystalline polymer, in addition to its non-toxicity and biocompatibility. It has good chemical and mechanical stability with outstanding applications such as oxygen barrier property, biosensors, drug delivery, selective permitted membranes, biomaterials, and immobilization of enzymes (Fahmy et al., 2020; Aziz et al., 2020a, 2020b; Nofal et al., 2020; Brza et al., 2021a, 2021b). Correspondingly, PVA able to react with various inorganic and organic materials through chemical and physical interactions due to its hydrophilic and polar properties of hydroxyl groups on alternate carbon atoms. Fahmy et al. (2021) were reported the polymer silane composites based on PVA-methoxy trimethyl silane. Their outcomes have shown that the addition of methoxytrimethylsilane (MTMS) has improved the refractive index, thermal and mechanical properties of the composite films (Fahmy et al., 2021). The optical band gap for the composite system based on the PVA-Al^{3+}-metal complex was also observed to decrease significantly as documented by Aziz et al. (2021). The existence of polar groups with high electron affinity in polar polymers are crucial to form coordination with cation or surface groups of the filler, resulting in the formation of homogenous composites (Aziz et al., 2021a). PVA assists the polymer composite formation due to its carbon chain backbone with an attached hydroxyl group that can be assumed as a precursor of hydrogen bonding.

Earlier reports have shown that the PVA polymer efficiently protects composites from aggregation (Nimrodh Ananth et al., 2011; Ghanipour and Dorranian, 2013). Moreover, previous studies have revealed the possibility of electronic interaction between the metal complex and the host polymer, which increase absorption intensity (Nimrodh Ananth et al., 2011; Ghanipour and Dorranian, 2013). Thereby, metal ions react with polymeric ligands comprising pendant functional groups that serve as chelating groups in binding polyvalent metal ions. This will lead to the formation of coordinated systems that could have increased chemical resistance as well as thermal stability. Azo compounds are of great interest due to their containing nitrogen, sulfur, and

oxygen donor atoms that have high versatility as ligands. The presence of many potential donner atoms is azo compounds, provides the flexibility and the ability to coordinate in either neutral and deprotonated form (Diab et al., 2018).

In the present study, the synthesis of the Hg metal complex will be explained based on coordination chemistry. The synthesized metal complex was added to the PVA host polymer via the solution cast technique to fabricate polymer composites. The impact of the used metal complex on the structural and optical properties of the host polymer will be thoroughly studied.

2. Materials and methods

2.1. Materials

Polyvinyl alcohol (PVA) powder with an average molecular weight of (85,000–124,000) g/mol was purchased from Sigma Aldrich. Ammonium pyrrolidine dithiocarbamate was obtained from Fluka Company. Ethylenediamine, Mercuric Chloride, Potassium hydroxide, and 3-chloro-2-butanone were purchased and used without further purification from Sigma Aldrich, BDH, Merck, and ACROS Organics companies, respectively.

2.2. Characterization techniques

The Identification of the Ligand and its complex were carried out by using Perkin-Elmer FTIR spectrometer in the (400–4000 cm^{-1}) range using KBr pellets (vmax in cm^{-1}). The electronic spectrum of the complex in DMSO and UV–visible spectra of the PVA composite film were measured using the absorbance mode of Jasco V-570 Ultraviolet (UV)-visible (Vis)-near-infrared (NIR) spectrophotometer.

The X-ray diffraction (XRD) pattern of the samples were achieved using Siemens D-5000 X-ray diffractometer (Bruker AXS GmbH, Berlin, Germany) at the wavelength (λ) of 1.5406 Å with 40 mA operating current and 40 kV voltage. The 2θ angle ranging from 10 to 80° with a step size of 0.1° was employed to scan the samples in the step-scan mode.

Thermal gravimetric analysis was measured using Perkin Elmer Diamond TG/DTA (SII) thermal analyzer. The condition was as follows: heating rate 10 °C/min in an air environment. The conductivity of the metal complex was obtained in DMSO using Fisher scientific Multimeter model XL600. Melting points of the complex were carried out on Electrothermal digital melting point apparatus Model 1102D.

2.3. Preparation of ligand

The HDBC [(3E,3′E)-(ethane-1,2-diylbis(azaneylylidene))bis(butan-2-yl-3-ylidene) bis(pyrrolidine-1-carbodithioate)] ligand was prepared by four consecutive steps. The first step involved adding ethylenediamine (0.01 mol, 0.601 g) drop by drop (very slowly due to its explosive nature) to a mixture of 3-chloro-2-butanone (0.022 mol, 2.343 g) and 1 mL ethanol in an ice bath and stirred continuously for about 15 min until the dark red viscous solution was formed. The second step comprises three times washing the dark red viscous liquid using diethyl ether. In the third step, ethanol was used to dissolve the viscous

product then was added to a refluxed solution of ammonium pyrrolidine dithiocarbamate (0.02 mol, 3.2858 g) in basic ethanol (0.021 mol, 1.176 g KOH). The mixture was refluxed continuously for about 24 h to prevent evaporation. In the final step, a rotary evaporator was used to evaporate the solvent so as to attain a black viscous product.

2.4. Preparation of Hg (II) metal complex and polymers composite

The mercury complex was prepared by adding a solution of (0.0015 mol, 10 mL EtOH) of the metal salt to a ligand solution of (0.0015 mol, 0.6865 g) as shown in Fig. 1. The mixture was refluxed for approximately 7 h. After that, the obtained product was filtered using filter paper and washed using ethanol and diethyl ether. The washed HgLCl$_2$ (L = C$_{20}$H$_{34}$N$_4$S$_4$) was dispersed in distilled water. Eventually, one gram of PVA was dissolved in 40 mL of distilled water (2.5% PVA) followed by stirring for around 1 h at 80 °C. The PVA solution was left to cool down to room temperature for about 2 h. The prepared HgLCl$_2$ metal complex was added to the PVA solution under continuous stirring to organize PVA composite, using a solution casting technique. The pure and doped PVA samples with Hg (II) metal complex were coded as SPNC-0 and SPNC-1, respectively.

3. Results and discussion

3.1. Study of FTIR spectroscopy and XRD analysis

All frequencies of the main characteristic bands of the Ligand and its complex were presented in (Table 1), and the FTIR spectrum with their description and assignments are shown in (Figs. 2 and 3). The band presence of the azomethine C=N, C—SS, N—CSS at 1604 cm^{-1}, 997 cm^{-1}, 1535 cm^{-1}, respectively are robust evidence on the ligand formation (McCormick, 1968). The wavenumber shift from 1325 to 1383 cm^{-1} can be resulted from the occurrence of Hg=S binding. Moreover, the intensity variation of some of these bands in the mercury complex spectrum is a clear indication of the formation of ligand metal bonds (Hadi et al., 2020). It is obvious that the frequency of C=N of the Schiff base group was shifted to the lower frequency in the complex from 1604 cm^{-1} to 1573 cm^{-1}. On another side, the peak of the M—N bond was observed at 518 cm^{-1} in the complex FTIR spectrum (Sari and Gürkan, 2004). The dithiocarbamate moiety was not coordinated with the mercury (II) ion in the complex, since there is no shift in the frequency of its bands.

The bands observed for the ligand spectra in the region of 2800–3000 cm^{-1} could be attributed to the symmetric —CH$_2$ stretch vibrations of the ligand. However, in the complex spectra, no shifts are observable, which demonstrates the —CH$_2$ is not participating in coordination (Fahmy et al., 2021, 2020). Additionally, the hydrated water molecule band cannot be seen in the spectrum of the complex (Dianu et al., 2010). The extended IR characteristics of at least two peaks in 3239–3408 cm^{-1} for [HDBC] ligand reflect the free C—OH stretches of hydroxyl in structures. These bands are subjected to a shift to 3226–3418 cm^{-1} in the [HgCl$_2$L] complex spectra and followed by an extensive decrease of intensity. These
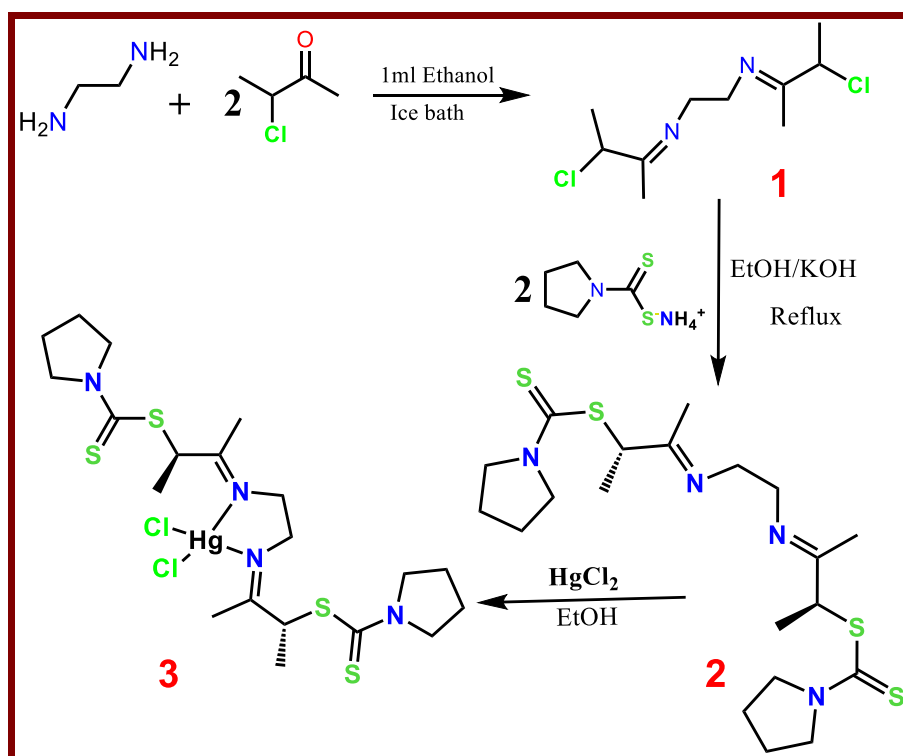
Fig. 1 Schematic illustration of the mercury complex [HgLCl$_2$] preparation.

Table 1 Frequencies of the main characteristic bands of the Ligand and its complex, where $_{S.b}$ stands for the Schiff base.

Compounds	C=N	C—SS	Hg=S	C—N $_{S.b}$	N—CSS	O—H(H$_2$O)	M—N	M—Cl
Ligand Spectrum (cm^{-1})	1604	997	1325	1406	1535	3408	–	–
[Hg(HDBC)] Spectrum (cm^{-1})	1573	994	1383	1442	1573	3418	518	–

regions are caused by a variety of probabilities, such as (1) it is owing to either free NH or OH groups; (2) it represents the strong hydrogen bonding interactions in the prepared complex between OH and NH groups; (3) presence of coordinated water molecules (Fahmy et al., 2020; Aziz et al., 2021b; Morgan et al., 2018). The band observed at 1383 cm^{-1} in the [HgCl$_2$L] complex spectra could be assigned to either —OH deformation of (H$_2$O) molecule, and Hg binding to =S (Yosef et al., 2020). In the complex of [HgCl$_2$L], each mercury atom is coordinated by two nitrogen atoms of the ligand. Therefore, the charges of the metal ion were neutralized by two coordinated chloride ions (Lahneche et al., 2019).

The FTIR spectra for pure PVA and the prepared PVA composite are presented in Fig. 4. In case of pure PVA the characteristic of C—O—H stretching vibration is related to the peak at 1075 cm^{-1} (Brza et al., 2021b). Additionally, there is a C=O and C=C stretching vibration that believed to be originated from acetate group, and located the peak of pristine PVA at around 1650 cm^{-1}, which is the inherent part of PVA (Aziz et al., 2021a). There is a clear peak occurs at 2910 cm^{-1}, which represent the band corresponds to C—H asymmetric stretching vibration (Brza et al., 2021b; Ghanipour and Dorranian, 2013). The O—H stretching absorption of hydroxyl groups can be related to a broad and robust absorption peak

at 3350 cm^{-1}, that corresponds to both intra and inters types of hydrogen bonding (Aziz et al., 2021a; Ghanipour and Dorranian, 2013). It is worth mentioning that there is a clear reduction in peaks intensity with band shifting up on the addition of the Hg metal complex to the pure PVA host matrix. The shifts and decline in intensities of the bands signifies a clear electrostatic interaction between the hydroxyl functional groups of PVA with the Hg metal complex (Brza et al., 2021b; Aziz et al., 2021a). This will result in binding of metal complex with the functional groups which lead to the larger molecular mass and cause the decline in vibrational intensity (Brza et al., 2021b; Aziz et al., 2021a). Eventually, the FTIR spectra of the doped PVA has shown a clear shift and drop in intensity compared to the pure PVA.

X-ray diffraction is considered as an accurate and direct technique to study the structural properties of the polymer composites (Nofal et al., 2020). The XRD pattern for pure and doped PVA samples are shown in Fig. 5. It can be noted that the pure PVA exhibit two clear peaks at around $2\theta = 19.65°$ and $41.15°$. It has been established that these peaks are attributed to the crystalline nature of PVA (Aziz et al., 2021a; Ghanipour and Dorranian, 2013). Up on the addition of Hg metal complex to the PVA polymer a clear reduction in the peaks intensities and broadening can be
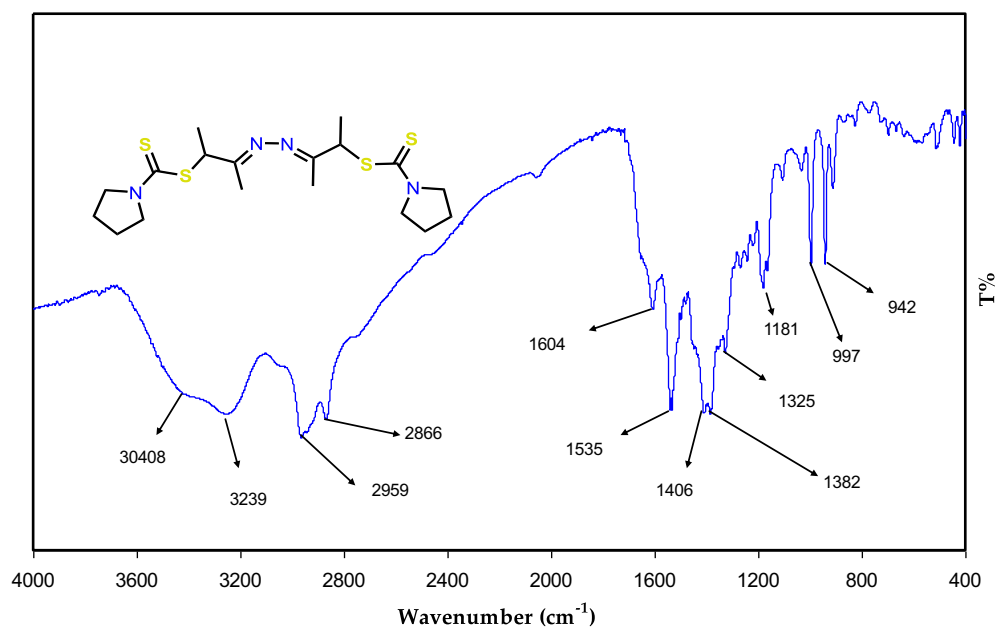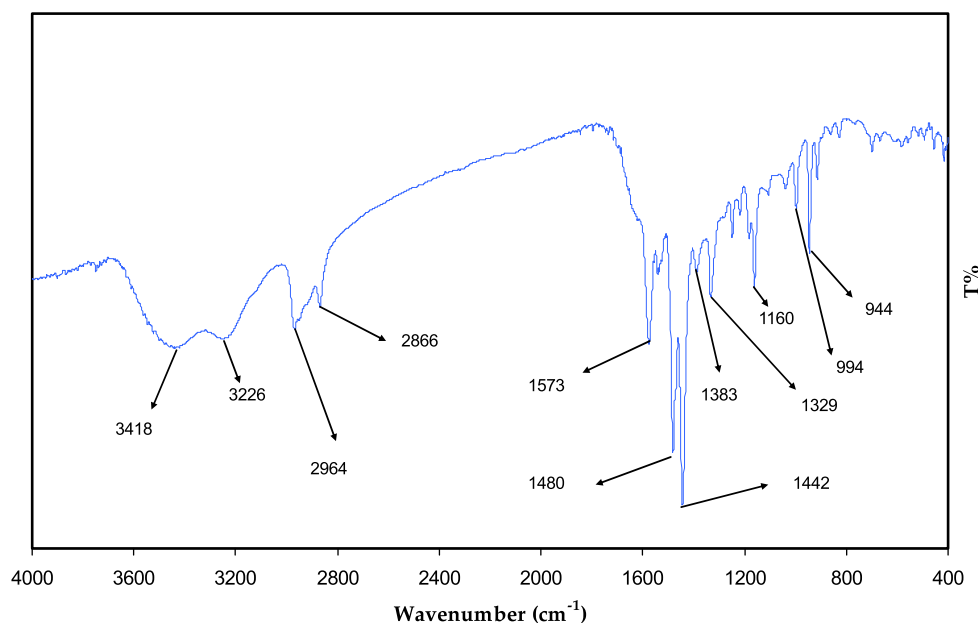
Fig. 2 FTIR Spectrum for [HDBC] Ligand.

Fig. 3 FTIR Spectrum for [Hg L Cl$_2$] Complex.

observed, particularly the peak at 41.15°, which is almost disappeared for the doped sample. Both peak intensity drop and widening are a clear indication of increased amorphous phase within the host PVA polymer (Aziz et al., 2020a; Nofal et al., 2020). This can be caused by the hydrogen bond disruption by the Hg metal complex and weakening intermolecular forces within the host polymer (Aziz et al., 2020b; Brza et al., 2021a, 2021b; Fahmy et al., 2021). The existence of crystalline peak after $2\theta = 19.65°$ even after the addition of metal complex highlights the semi-crystalline structure of prepared composite. These outcomes reveal the impact of Hg metal complex

on enhancing the amorphous nature of the PVA host polymer, however some original crystalline features still exist.

3.2. UV–visible spectroscopy

When a light in the ultraviolet and visible region is absorbed by a material, it results in electron promotions from lower to the higher excited state in σ, π and n-orbitals, as stated in molecular orbital theory. Accordingly, $\sigma \rightarrow \sigma^*$, $n \rightarrow \pi^*$, $\pi \rightarrow \pi^*$ transitions will occur (Aziz et al., 2019; Sarma and Das, 2013). The UV–visible spectra of the Hg (II) metal
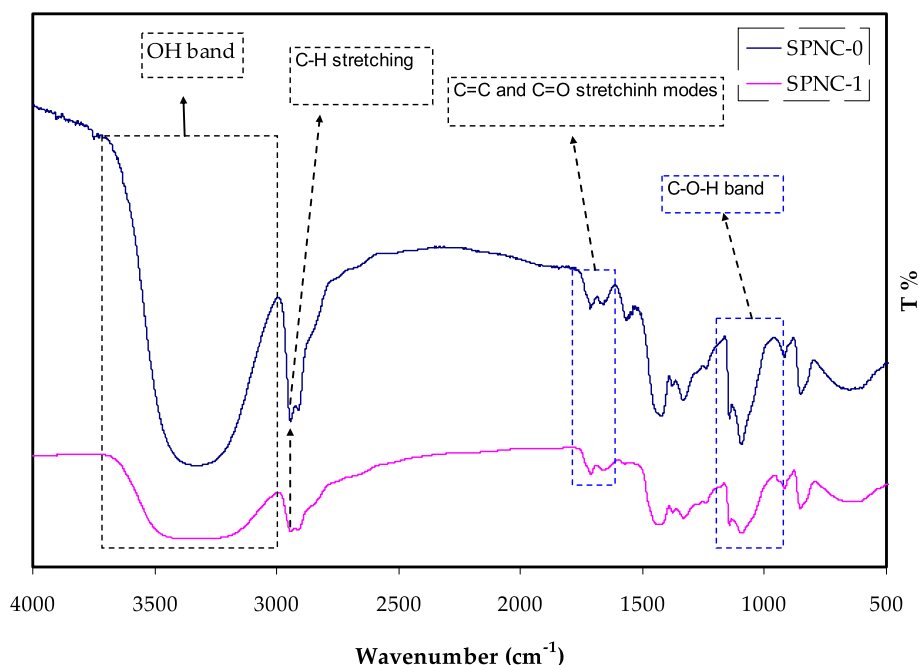
Fig. 4   FTIR Spectrum for the pure and doped PVA with Hg metal complex.
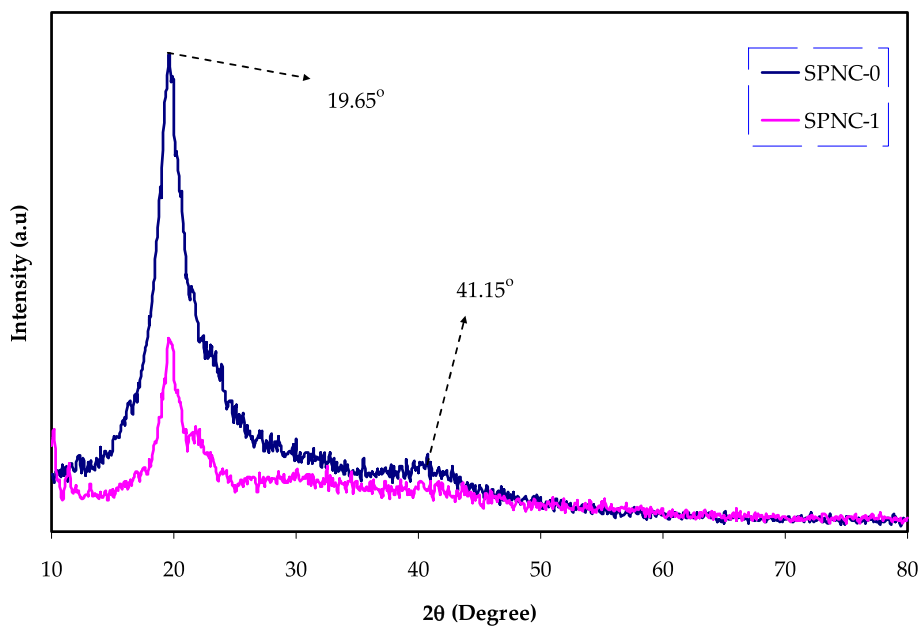

Fig. 5   XRD pattern of pure PVA and doped PVA with Hg (II) metal complex.

complex was recorded in the solvent of dimethyl sulfoxide (DMSO). The variation of absorption spectrum against wavelength achieved for the Hg metal complex is shown in Fig. 6. It can be witnessed that the absorption edge is dropped sharply in the range of about 260–300 nm, and shifted to the higher wavelengths. This is signifying the presence of the Hg metal complex. It is noteworthy to mention that the Hg metal complex displayed a broad peak around 325–375 nm along with the wavelength region (Abdullah et al., 2015). This is related to the collective oscillation of conduction electrons in response to the applied electromagnetic field, which is commonly known as the surface plasmon resonance (SPR) (Aziz et al., 2010). The UV–Visible spectrum of the complex displays only two bands in the region of 263 and 354 nm, arisen from the charge transfer band (Lahneche et al., 2019). Additionally, it should be noted that the entire visible range is enclosed by the spectrum of absorption as it begins in the visibility range and ends in the UV range (Xu et al., 2014). An earlier study has reported the SPR in the wavelength range of 500–800 nm due to the copper nanoparticles (Aziz, 2017; Zulkifli et al., 2020). Thus, the broad absorption ranges from 325 nm to 400 nm may be ascribed to a free-electron oscillation of the Hg metal complex.
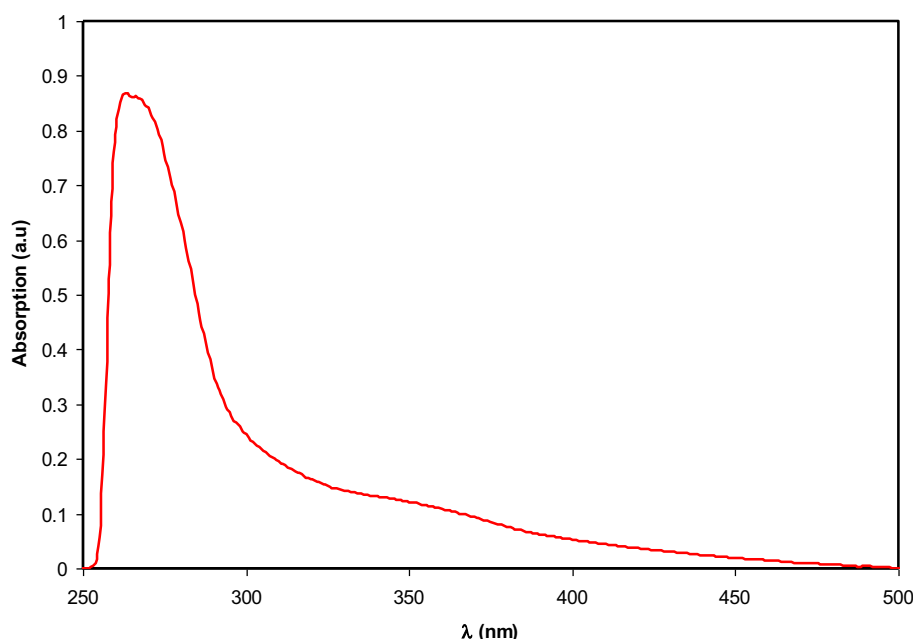
Fig. 6 Absorption spectrum for colloidal suspension of Hg^{2+}-metal complex.

3.3. Thermal study

Fig. 7 show the TG curves for the ligand and Hg metal complex, at the temperature range of between 40 and 600 °C (El-Sonbati et al., 2018). Two major stages are correlated with loss of ligand molecule, while three main steps can be observed for the Hg metal complex. This could be attributed to the loss of uncoordinated water H_2O molecule in addition to a part of coordinated H_2O. The 2nd and 3rd steps demonstrate the loss of other molecules of the coordinated H_2O, followed by the decomposition of the final components of the Hg metal complex (El-Sonbati et al., 2019; Morgan et al., 2018). Overall, the complex thermal analysis spectra show high thermal stability. The TG curve displayed the initial weight loss of the ligand

up to about 100 °C. Therefore, the loss in mass of the complex close to zero until around 200 °C, and then it begins to decompose at 210 °C. Then, it continued until the temperature of 300 °C. This could be owing to the decomposition of the water, ligand, and complex (Kavitha and Anantha Lakshmi, 2017; Jiang et al., 2011; Sekerci and Yakuphanoglu, 2004; Kesavan et al., 2014).

3.4. Absorption study

UV–Vis spectroscopy is considered as an effective technique to determine the electronic transitions and study the optical properties of the polymer nanocomposite samples over a wide range of wavelengths. This work recorded a substantial enhancement
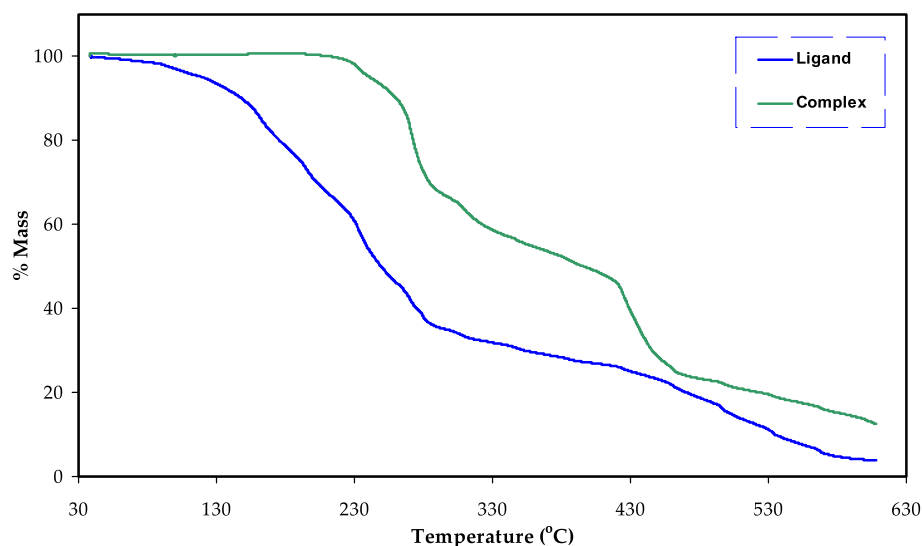

Fig. 7 TG curve for the ligand and Hg metal complex.

in the optical absorption upon the addition Hg (II) complex. The absorption pattern of pure PVA (SPNC-0) and doped PVA films with metal complex (SPNC-1) are depicted in Fig. 8. Both improved absorption with a significant reduction in the band gap of PVA host are related to the generation of new energy levels in the prohibited gap of the polymer upon the addition of metal complex (Abdul-Kader, 2013; Aziz et al., 2017a, 2013). The impact of the Hg (II) metal complex on the pure PVA can be documented via this shifting to a longer wavelength (i.e. lower energy) in the UV spectra. It can be seen that a noteworthy absorption at longer wavelengths take place as shown in Fig. 8. All these confirm the viability of these raw materials for organic solar cell and optoelectronic device applications, due to their wide range absorption spectrum, and reduced band gap. The doped sample exhibited an exponential behavior in the absorption pattern compared to the pure PVA.

The analysis of variation in absorption spectra can be used to extract the kind of electronic transition that occurs within the materials. The sharp increase in absorption pattern is basically related to the exciting or band to band transitions, which is known as absorption edge. It is usually a good denoting of the optical energy gap (Brza et al., 2020; Aziz et al., 2017b). The amount of absorption is based on the attenuation rate of incident light in a unit length of a medium, which is called absorption coefficient $\alpha(\upsilon)$ (Elimat et al., 2008; Abdullah et al., 2019; Aziz et al., 2015). The quantitative relationship between absorbed light and concentration can be represented via Beer-Lambert law (Abdullah et al., 2019). From this law the absorption spectrum $A(\upsilon)$ can be used to calculate the $\alpha(\upsilon)$ at the given wavelength (or frequency (υ)) as follow (Abdullah et al., 2019):

$$\alpha(v) = \frac{2.303}{d} \log\left(\frac{I_o}{I}\right) = \frac{2.303}{d} A(v) \qquad (1)$$

where the incident and transmitted light intensities are denoted by I_o and I; respectively, and d is the thickness of the sample. The trends of variation in $\alpha(\upsilon)$ as a function of photon energy
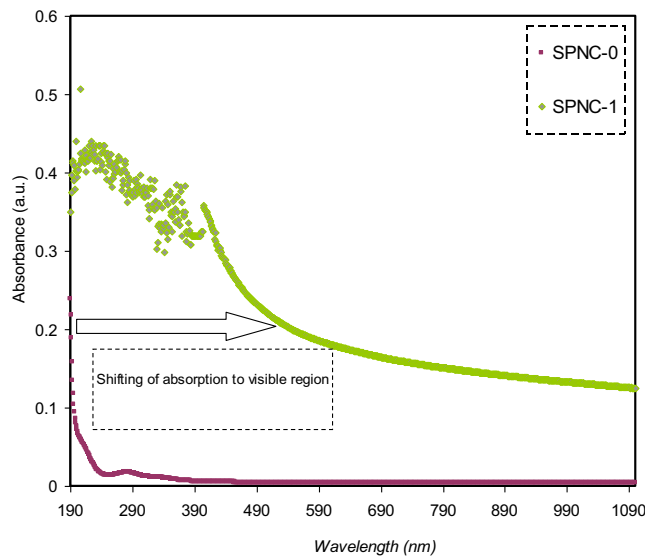
($h\upsilon$) for pure and doped PVA film with metal complex (MC) are presented in Fig. 9. The spectra of the absorption coefficient for the pure PVA exposed two peaks in the UV–visible region; while, only a peak is observed for the composite sample in the visible region. This is due to the molecular orbital transition from bonding to antibonding molecular orbitals (El-Ghamaz et al., 2017). The band is appearing at around 5 eV and the shoulder at about 3.5 to 4.5 eV for the SPNC-0 sample are assigned to $\pi \rightarrow \pi^*$ and $n \rightarrow \pi^*$ transitions between orbitals mostly localized ring. The different forms of transitions are due to either donating or withdrawing functional groups. The inclusion of the chromophore units such as C=O, C=C, and C—O effects the intensity of the $\pi \rightarrow \pi^*$ plasmon peaks (Yosef et al., 2020). The amorphous nature of the samples is responsible for the presence of the tail (El-Ghamaz et al., 2012). One can notice that upon the addition of MC the absorption edge is shifted from 6.2 eV for pure PVA to 1.43 eV for the doped PVA. This has resulted from the band structure modification (establishment of new energy levels) in the pure PVA (Aziz, 2017). As a consequence, the addition of MC into the PVA matrix has dropped the value of band gap energy significantly.

3.5. Refractive index (n)

Fig. 10 shows the effect of Hg (II) complex addition on the refractive index of PVA host polymer. It is observed that the samples possess a wide dispersion region and relatively high refractive index over a broad range of wavelengths. Recently, the focus has been devoted to examining relatively high refractive index polymers due to their promising applications in various display units like advanced organic light-emitting diodes (OLEDs), antireflection coatings, and different semiconductors (Asai et al., 2011; Hussein et al., 2020). The attempts have been concentrated on enhancing the refractive index of polymers by different means, including insertion of perfluorocyclobutane and adamantan, and sulfur atom groups into
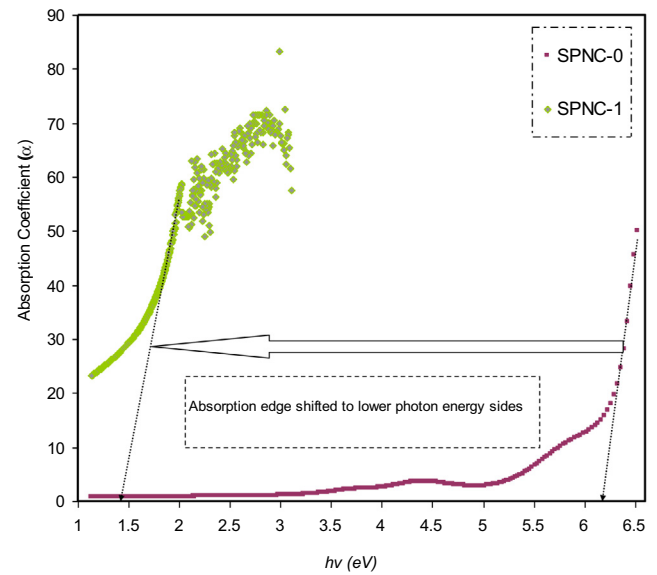

Fig. 8 The absorption pattern of pure and doped PVA films with the metal complex.
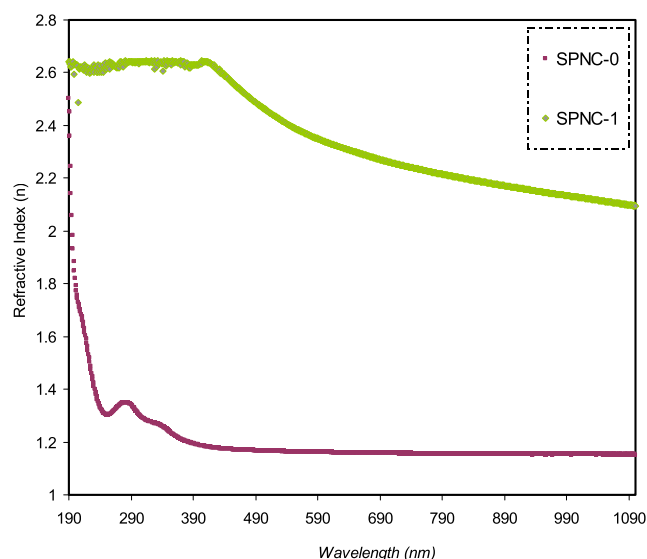

Fig. 9 Absorption coefficient plot for pure and doped PVA films with the metal complex.

Fig. 10 Refractive index pattern for pure and doped PVA films with the metal complex.

Table 2 Refractive index values of various polymer composite systems.

Composition	Refractive index	Ref.
PVA: DMDMS	1.35	Fahmy et al. (2020)
PS: SnTiO$_3$	2.6	Hussein et al. (2020)
PVA:PVP:Ag$_2$S	1.52	Aziz et al. (2017c)
PVA:Al	2.14	Aziz et al. (2017d)
PMMA: ZnO	~1.65	Wang et al. (2017)
PGMA: TiO$_2$	1.8	Tao et al. (2011)
PEO: SnTiO$_3$	2.47	Muhammed et al. (2020)
PVA: Hg-metal complex	2.15	Present work

Where, DMDMS = dimethoxy dimethyl silane.

polymers, in addition to the use of organic/inorganic dopants (Seto et al., 2010; Hussen, 2020). The refractive index is an effective property of materials to be utilized in optoelectronic and photonic devices and especially in organic solar cells (OSCs). This property is essential to realize the way of optimizing the performance of photovoltaics (Campoy-Quiles et al., 2014). The literature has confirmed that particular materials with a high refractive index are found to be eligible for organic solar cell applications (Muhammad and Sulaiman, 2011). The refractive index (*n*) of PVA obtained in the present work is higher than those reported for PVA by ion incorporation in the literature (Stoyanov et al., 2012).

Shi et al. studied nonlinear optical (NLO) polymers such as polyether ketone (PEK-c) with *n* value which is lower than the observed wide dispersion for the material under study (Shi et al., 1999). This indicates the importance of these materials for the realization of integrated-optic devices such as electro-optic modulators and switches. The refractive index (*n*) value obtained in this study is comparable with the previous works of polymer composites. Fahmy et al. (Fahmy et al., 2021) were documented the refractive index value of 1.34 for the system of PVA: MTMS based polymer composite, where (MTMS = methoxy trimethyl silane). Table 2 compares the refractive index of the current study which is higher than many other polymers impregnated with various fillers. This outcome highlights the vital role of the used meal complex on improving the refractive index of the polymer composite.

It is crucial to investigate one of the most important parameters that give useful information about the material's electric properties, which is known as the dielectric constant (El-Ghamaz et al., 2017). This work also studied the optical dielectric constant of the samples including both real ($\varepsilon_r = n^2 - k^2$) and imaginary ($\varepsilon_i = 2nk$) parts. These provide insight into the energy density state in the optical band gap of the films (Caglar et al., 2006; Aziz et al., 2019). The dielectric function cannot be measured directly from an experiment using optical spectroscopy. Different optical parameters are measured, such as refractive index, absorbance, reflectance,

and extinction coefficient. The optical dielectric constant plot of the PVA-based composite samples is exhibited in Fig. 11. In fact, there is a strong correlation between dielectric function and the band structure of the material. The overall image of the band structure of a material can be predicted using the study of dielectric function from optical spectroscopy (Steyl, 2009; Aziz et al., 2020c).

In Fig. 11 there is an increase of the dielectric constant with rising the quantity of MC. The rise of the dielectric constant proves the presence of a population of states of various energy densities, resulting in an increase in polarization. The dielectric constant shows a clear dispersion region at low wavelengths, while it is nearly constant at high wavelengths. The interaction of electromagnetic light with the material causes the internal charge structure to undergo temporal forces as a consequence of the impact of the electric field component of the incident wave. The noticed dispersion region is relatively wide, which could be owing to the polar nature of the samples. The worth-noting observation is that polar molecules are not able to follow fast field oscillation at high wavelengths because of
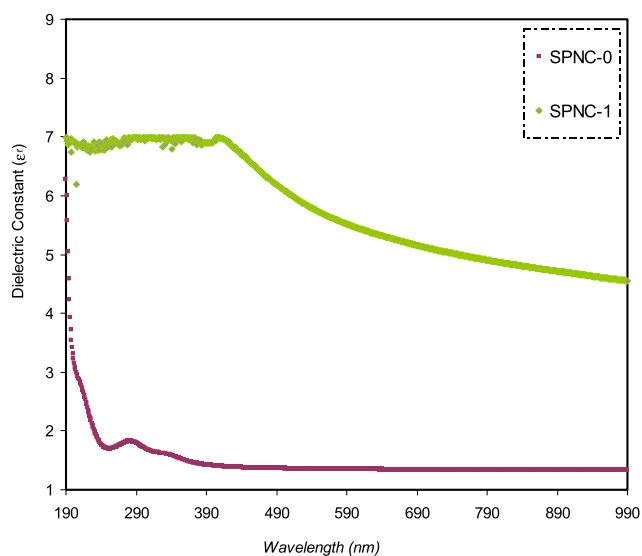

Fig. 11 The plot of ε_r as a function of wavelength for pure and doped PVA films with the metal complex.

their inertia (Hecht, 2002; Hadi et al., 2020; Hadi et al., 2020). Importantly, the dispersion in dielectric constant in the spectra indicates the eligibility of these materials to be utilized in optical communication applications and fabrication of optical devices (Muhammad and Sulaiman, 2011).

3.6. Band gap study

The imaginary part of the dielectric constant is illustrated in Fig. 12. Previous studies have established a substantial correlation between electronic band structure and optical properties of the materials (Aziz et al., 2017c; Taib et al., 2012). The wavelength-dependent complex dielectric function determines the characteristic optical properties of absorbing isotropic materials (Kymakis and Amaratunga, 2004). Using dielectric function (real and imaginary parts), one can easily specify optical functions that can be determined (Amin et al., 2018). In fact, the electronic polarizability is related to the real component ε_r; while, the ε_i is expressing the electronic absorption of the materials (Ben Nasr et al., 2013). The complex dielectric function usually provides information about the optical properties (Amin et al., 2018):

$$\alpha^*(\omega) = \varepsilon_r + j\varepsilon_i \tag{2}$$

The direct and indirect band gap transitions contribute mainly and partly in $\varepsilon_{(\omega)}$, respectively because these are mediated by phonons (Taib et al., 2012). Earlier studies demonstrated that the optical band gap can be accurately calculated from both KT and Tauc's equation (Aziz et al., 2017a, 2017b, 2017c; Thutupalli and Tomlin, 1976). Nevertheless, in the case of optical band gap investigation, a straightforward and accurate method has been established in data analysis (Aziz et al., 2019; 2017b, 2017c). It is thought that an accurate determination of the optical band gap can be achieved via optical dielectric loss. This is based on the development of various models and quantum mechanics for the band gap analysis. In order to characterize the electron-photon interaction within the material, the time-dependent

perturbations of the ground electronic state as a principle of quantum mechanics can be considered. For a transition to occur between occupied and unoccupied states, photon absorption or emission already takes place. The imaginary component ε_i is a complex mathematical expression of the dielectric function that possesses the following form (Aziz et al., 2019):

$$\varepsilon_i = \frac{2\pi e^2}{\Omega\varepsilon_0} \sum_{K,V,C} \left|\langle\psi_K^C|u \cdot r|\psi_K^V\rangle\right|^2 \partial(E_K^C - E_K^V - E) \tag{3}$$

where k and u are representing the reciprocal lattice vector and the vector characterizing the incident electric field polarisation, respectively. Both superscripts C and V are expressing the conduction band and the valence band, respectively, and the ω refers to the frequency of incident photon (Li et al., 2009).

Fig. 12 shows the imaginary part of the dielectric constant ε_i $_{(\omega)}$. An intersection from the linear region of the plot was drawn onto the x-axis in order to determine the optical band gap. This response of the optical spectra resulted from electrons movement from the highest point of valence bands to the lowest point of conduction bands. The optical energy gap can be recognized from the fundamental absorption edge, which is called absorption edge (Zhao et al., 2011). From the closeness and strong correlation of the points of significance, it is easy to determine band gap values (Cheddadi et al., 2017).

The inter-band absorption model can be employed to specify the nature of electronic transition within the band gap of materials. Based on the inter band absorption theory, photon causes electron excitation from the highest occupied energy level in the valence band to the lowest unoccupied energy level in the conduction band. The optical band gap of materials can be calculated from the following relationship (Kesavan et al., 2014; Aziz et al., 2017a):

$$\alpha h v = B(hv - E_g)^p \tag{4}$$

where B and E_g are energy-independent constant and the optical energy band gap, respectively, p is a constant from which one can determine the nature of the optical transition from the valence band to the conduction band (fundamental absorption).

In this work, p is equal to 1/2, indicating an allowed direct transition. In allowed direct transition, there is a direct vertical transition by an electron from the top of the valence band to the bottom of the conduction band; while normally the non-vertical transitions are not allowed (forbidden) (Kesavan et al., 2014).

Figs. 13–16 exhibit a correlation between $(h\alpha v)^2$ and hv for pure PVA and PVA doped samples. Generally, an extrapolation is drawn from the linear part of a plot to zero absorption in order to determine the optical band gap.

It is worth noting that the energy band gap of pure PVA is (5.38 eV), which is relatively considerably large compared to the other sample. In this work, the direct optical band gap of pure PVA was found to be in good accordance with that documented in the literature (Bhargav et al., 2007). From the perspective of solid-state physics, an energy band gap is an energy range in a solid that no electron states can exist. The band gap energy is the amount of energy required to remove an outer shell electron from its orbit and move freely within the materials. Thus, the band gap is the main barrier in determining the electrical conductivity of a solid. For example,
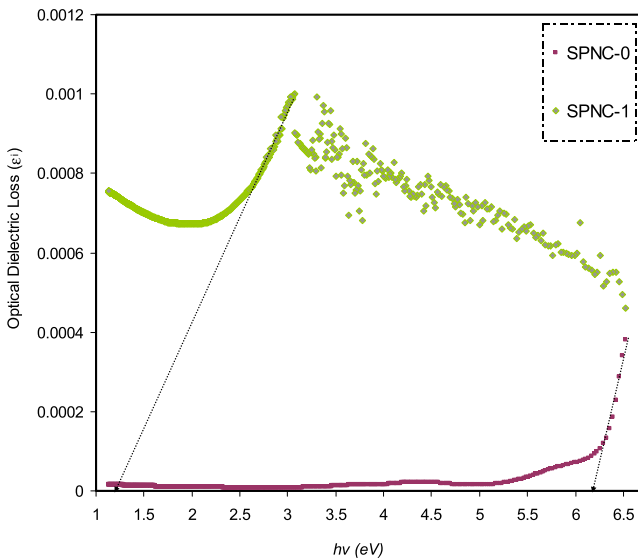
Fig. 12 Optical dielectric loss plot for pure and doped PVA films with the metal complex.
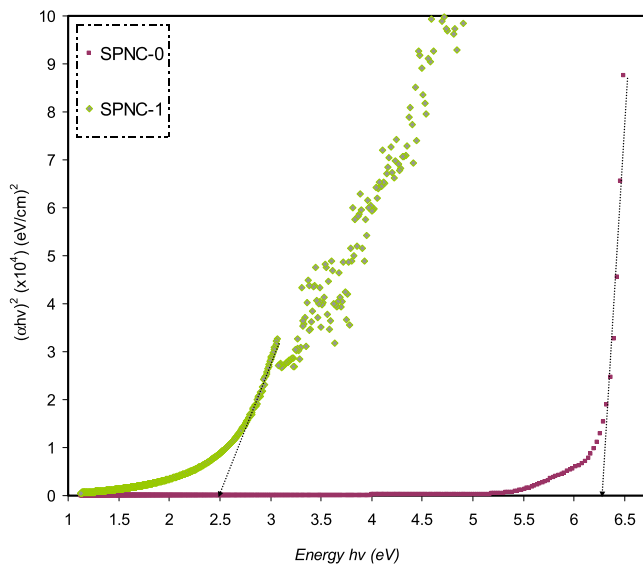
Fig. 13 $(\alpha h\nu)^2$ as a function of photon energy for the SPNC-0 and SPNC-1 films.
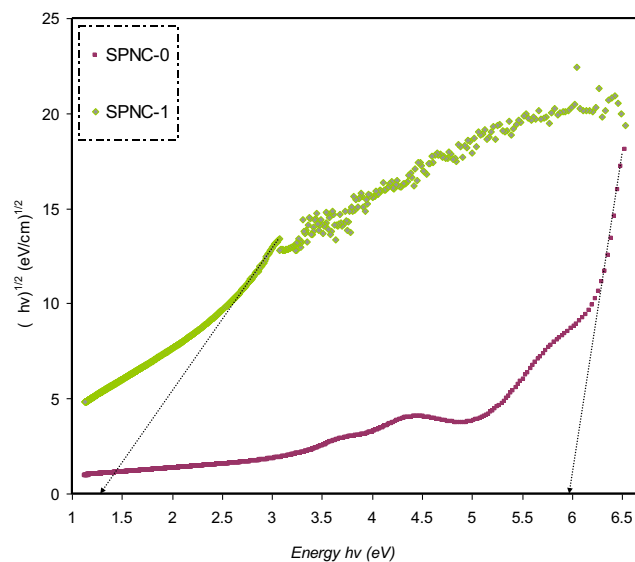

Fig. 15 $(\alpha h\nu)^{1/2}$ as a function of photon energy for the SPNC-0 and SPNC-1 films.
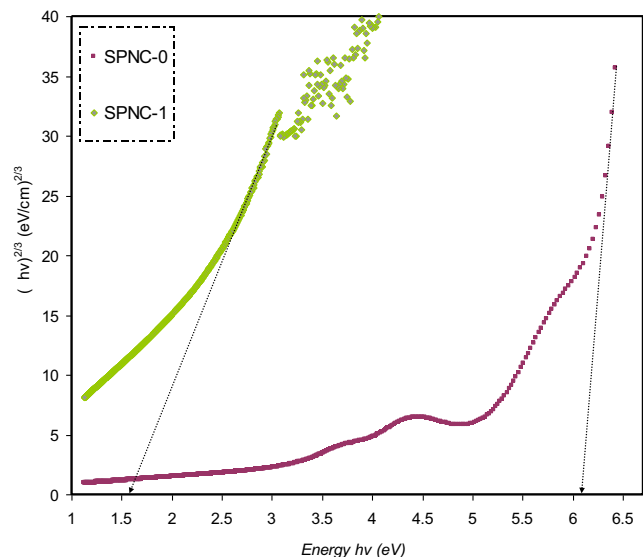

Fig. 14 $(\alpha h\nu)^{2/3}$ as a function of photon energy for the SPNC-0 and SPNC-1 films.
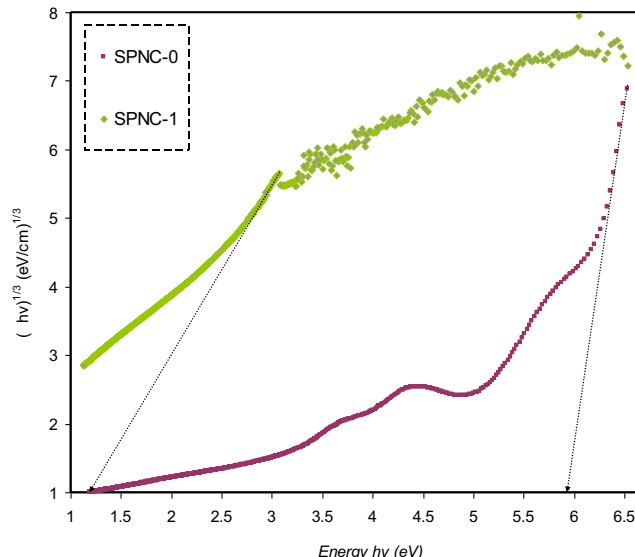

Fig. 16 $(\alpha h\nu)^{1/3}$ as a function of photon energy for the SPNC-0 and SPNC-1 films.

those materials that possess large band gaps are generally insulators and those relatively smaller band gaps are semiconductors. Based on this fact, the pure PVA is considered as an insulator with a wide band gap energy (5.38 eV). Importantly, in the present work, it has been realized that the optical band gap of pure PVA can be tuned so as to meet a specific requirement. In the current study this goal can be achieved through introducing a particular quantity of Hg (II) metal complex which is eligible for a specific application. As a measure, the narrow band gap indicates the ability of materials to compensate for the relatively low energy photon harvest (An et al., 2013).

Previous studies clarified that the plot of $(\alpha h\nu)^{1/2}$ and $(\alpha h\nu)^2$ as a function of photon energy (hν) can be used to verify the occurrence of both direct and indirect transitions near to the fundamental band edge (Mohan et al., 2007; Mohan et al., 2007). The exponent (p) value of Tauc's equation can be obtained from the plot of $(\alpha h\nu)$ against photon energy (hν) as shown in Figs. 13–16. It can be noticed that the linear parts were obtained from each plot and the intersections on the x-axis were used to compute the optical energy band gaps. In amorphous materials, the indirectly allowed transitions are employed in the analysis of the absorption edge, as indicated from the theory of the electronic structure of amorphous materials (Edukondalu et al., 2015). The power coefficient value indicated by the parameter p is determined depending on the forms of possible electronic transitions that are p is equal to 2 and 1/3 for indirect allowed and forbidden, respectively, and p is equal to 1/2 and 2/3 for direct allowed and forbidden,

Table 3 Optical dielectric loss and optical band gap from Tauc's model.

Sample code	E_g (eV) for $p = 2$	E_g (eV) for $p = 2/3$	E_g (eV) for $p = 1/2$	E_g f(eV) for $p = 1/3$	E_g from ε_i $(h\nu)$ plot
SPNC-0	6.3	6.1	5.95	5.9	6.2
SPNC-1	2.5	1.6	1.3	1.2	1.2

Table 4 PVA band gap variation incorporated with different fillers and nanoparticles.

PVA Composite	Direct band gap (eV)	Indirect band gap (eV)	Reference
PVA: Ag	–	4.78	Ghanipour and Dorranian (2013)
PVA: Ni	5.15	3.4	Soliman et al. (2020)
PVA: Al3 + -complex	1.81	1.62	Aziz et al. (2021)
PVA: MnCl2	4.99	4.93	Banerjee et al. (2019)
PVA: HgS	4.88	–	Abdullah et al. (2015)
PVA: Hg-complex	**1.3**	**1.2**	**This work**

respectively. The optical band gap from Tauc's model for p is equal to 2, 1/3,1/2, and 2/3, and optical dielectric loss values is summarized in Table 3.

Obviously, the calculated band gap values for PVA doped samples for p is equal to 1/3 (i.e., indirect forbidden) is sufficiently near to the calculated band gap magnitudes achieved from the plot of optical dielectric loss, as shown in Table 3. As a consequence, the reduced crystalline order in the PVA doped film is linked to the direct forbidden (i.e., p is equal to 2/3) results for the hybrid sample. The optical band gap obtained from Figs. 13–16 for the various value of p from Eq. (4) as a comparison to the E_g value achieved from the plot of optical dielectric loss suggests the direct allowed (i.e., p is equal to 1/2) of electronic transition in the PVA. In fact, in amorphous materials, the most probable type of transition is considered to be indirect. In indirect band gap materials, the transition from the valence band to the conduction band is based on having a phonon with the right magnitude of crystal momentum (Brza et al., 2019; Mohan et al., 2007). It is difficult to identify the value of p because of the considerable fluctuation in the values of the achieved optical band gap. Consequently, the type of conduction mechanism can be specified using Eq. (4). The actual E_{opt} determination depends on another factor, which is the imaginary part (ε_2) of the dielectric constant. From this, one can select exponent value accurately (Edukondalu et al., 2015) (see Table 4).

4. Conclusion

In conclusion, a flexible polymer composite based on the PVA doped with Hg (II) metal complex has been fabricated. Various spectroscopic techniques were employed for characterization of the prepared Hg (II) metal complex. The shift and intensity drop of the FTIR spectra revealed a good complexation between the dopant and host matrix. The enhanced amorphous nature of the polymer composite resulted from the interaction between the functional groups of the host polymer with Hg metal complex and it was docu-

mented from the XRD patterns of the samples. It has been confirmed that the surface plasmonic resonance (SPR) peak in the absorption spectra of the doped sample was originated from the Hg (II) metal complex. The optical band gap substantial reduced from 6.2 eV to 1.4 eV, which signified the occurrence of interaction between the Hg (II) complex and the PVA matrix. The formation of new energy states with reduced energy band gap is evidenced by the increment in the refractive index upon the addition of the metal complex. Moreover, shifting of absorption edge to smaller photon energy confirmed the effect of the Hg (II) on the optical band gap of the host PVA. Strong absorptions in the region of 263 nm and 354 nm were assigned to the $n \rightarrow \pi^*$, $\pi \rightarrow \pi^*$ transitions. Through investigating Tauc's model, it was concluded that the samples exhibited an indirect forbidden transition. The broad absorption ranged from 325 nm to 400 nm may be ascribed to a f ree-electron oscillation of the Hg metal complex.

5. Author agreement

All authors agree to submit and publish this work. The article has been written by the stated authors who are ALL aware of its content and approve its submission.

Declaration of Competing Interest

The authors declare that they have no known competing financial interests or personal relationships that could have appeared to influence the work reported in this paper.

References

Abdul-Kader, A.M., 2013. The optical band gap and surface free energy of polyethylene modified by electron beam irradiations. J. Nucl. Mater. 435, 231–235. https://doi.org/10.1016/j.jnucmat.2013.01.287.

Abdullah, O.G., Aziz, S.B., Omer, K.M., Salih, Y.M., 2015. Reducing the optical band gap of polyvinyl alcohol (PVA) based nanocomposite. J. Mater. Sci. Mater. Electron. 26, 5303–5309. https://doi.org/10.1007/s10854-015-3067-3.

Abdullah, R.M., Aziz, S.B., Mamand, S.M., Hassan, A.Q., Hussein, S. A., Kadir, M.F.Z., 2019. Reducing the Crystallite Size of Spherulites in PEO-Based Polymer Nanocomposites Mediated by Carbon Nanodots and Ag Nanoparticles. Nanomaterials 9, 874. https://doi.org/10.3390/nano9060874.

Abdullah, Omed Gh., Salman, Yahya A.K., Saleem, Salwan A., 2015. In-situ synthesis of PVA/HgS nanocomposite films and tuning optical properties. Phys. Mater. Chem. 3, 18–24. https://doi.org/10.12691/pmc-3-2-1.

Abu-Dief, A.M., Mohamed, I.M.A., 2015. A review on versatile applications of transition metal complexes incorporating Schiff bases. Beni-Suef Univ. J. Basic Appl. Sci. 4 (2), 119–133. https://doi.org/10.1016/j.bjbas.2015.05.004.

Amin, P.O., Kadhim, A.J., Ameen, M.A., Abdulwahid, R.T., 2018. Structural and optical properties of thermally annealed TiO2–SiO2 binary thin films synthesized by sol–gel method. J. Mater. Sci. Mater. Electron. 29, 16010–16020. https://doi.org/10.1007/s10854-018-9688-6.

An, Q., Zhang, F., Zhang, J., Tang, W., Wang, Z., Li, L., Xu, Z., Teng, F., Wang, Y., 2013. Enhanced performance of polymer solar cells through sensitization by a narrow band gap polymer. Sol. Energy Mater. Sol. Cells 118, 30–35. https://doi.org/10.1016/j.solmat.2013.07.050.

Asai, K., Konishi, G.I., Sumi, K., Mizuno, K., 2011. Synthesis of silyl-functionalized oligothiophene-based polymers with bright blue light-emission and high refractive index. J. Organomet. Chem. 696, 1236–1243. https://doi.org/10.1016/j.jorganchem.2010.11.013.

Aziz, S.B., 2017. Morphological and optical characteristics of chitosan (1−x): Cuox (4 ≤ x ≤ 12) based polymer nano-composites: Optical dielectric loss as an alternative method for tauc's model. Nanomaterials 7, 1–15. https://doi.org/10.3390/nano7120444.

Aziz, S.B., Abidin, Z.H.Z., Arof, A.K., 2010. Influence of silver ion reduction on electrical modulus parameters of solid polymer electrolyte based on chitosansilver triflate electrolyte membrane. Express Polym. Lett. 4, 300–310. https://doi.org/10.3144/expresspolymlett.2010.38.

Aziz, S.B., Hussein, S., Hussein, A.M., Saeed, S.R., 2013. Optical Characteristics of Polystyrene Based Solid Polymer Composites: Effect of Metallic Copper Powder. Int. J. Met. 2013, 1–6. https://doi.org/10.1155/2013/123657.

Aziz, S.B., Ahmed, H.M., Hussein, A.M., Fathulla, A.B., Wsw, R.M., Hussein, R.T., 2015. Tuning the absorption of ultraviolet spectra and optical parameters of aluminum doped PVA based solid polymer composites. J. Mater. Sci. Mater. Electron. 26, 8022–8028. https://doi.org/10.1007/s10854-015-3457-6.

Aziz, S.B., Abdulwahid, R.T., Rsaul, H.A., Ahmed, H.M., 2016. In situ synthesis of CuS nanoparticle with a distinguishable SPR peak in NIR region. J. Mater. Sci.: Mater. Electron. 27 (5), 4163–4171. https://doi.org/10.1007/s10854-016-4278-y.

Aziz, S.B., Rasheed, M.A., Ahmed, H.M., 2017a. Synthesis of Polymer Nanocomposites Based on [Methyl Cellulose](1−x):(CuS)x (0.02 M ≤ x ≤ 0.08 M) with Desired Optical Band Gaps. Polymers 9, 194. https://doi.org/10.3390/polym9060194.

Aziz, S.B., Mamand, S.M., Saed, S.R., Abdullah, R.M., Hussein, S.A., 2017b. New Method for the Development of Plasmonic Metal-Semiconductor Interface Layer: Polymer Composites with Reduced Energy Band Gap. J. Nanomater. 2017. https://doi.org/10.1155/2017/8140693.

Aziz, S.B., Rasheed, M.A., Hussein, A.M., Ahmed, H.M., 2017c. Fabrication of polymer blend composites based on [PVA-PVP](1−x):(Ag2S)x (0.01 ≤ x ≤ 0.03) with small optical band gaps: Structural and optical properties. Mater. Sci. Semicond. Process. 71, 197–203. https://doi.org/10.1016/j.mssp.2017.05.035.

Aziz, S.B., Abdullah, O.G., Hussein, A.M., Abdulwahid, R.T., Rasheed, M.A., Ahmed, H.M., Abdalqadir, S.W., Mohammed, A.R., 2017d. Optical properties of pure and doped PVA:PEO based solid polymer blend electrolytes: two methods for band gap study. J. Mater. Sci. Mater. Electron. 28, 7473–7479. https://doi.org/10.1007/s10854-017-6437-1.

Aziz, S.B., Hassan, A.Q., Mohammed, S.J., Karim, W.O., Kadir, M.F.Z., Tajuddin, H.A., Chan, N.N.M.Y., 2019. Structural and optical characteristics of pva:C-dot composites: Tuning the absorption of ultra violet (uv) region. Nanomaterials 9 (2), 216. https://doi.org/10.3390/nano9020216.

Aziz, S.B., Marif, R.B., Brza, M.A., Hassan, A.N., Ahmad, H.A., Faidhalla, Y.A., Kadir, M.F.Z., 2019. Structural, thermal, morphological and optical properties of PEO filled with biosynthesized Ag nanoparticles: New insights to band gap study. Results Phys. 13, 102220. https://doi.org/10.1016/j.rinp.2019.102220.

Aziz, S.B., Brza, M.A., Dannoun, E.M.A., Hamsan, M.H., Hadi, J.M., 2020a. The Study of Electrical and Electrochemical Properties of Magnesium Ion Conducting CS : PVA Based Polymer Blend Electrolytes: Role of Lattice Energy of Magnesium Salts on EDLC Performance. Molecules 25, 4503. https://doi.org/10.3390/molecules25194503.

Aziz, S.B., M. Hadi, J., Dannoun, E.M.A., Abdulwahid, R.T., R. Saeed, S., Shahab Marf, A., Karim, W.O., Kadir, M.F.Z., 2020b. The study of plasticized amorphous biopolymer blend electrolytes based on polyvinyl alcohol (PVA): Chitosan with high ion conductivity for energy storage electrical double-layer capacitors (EDLC) device application. Polymers (Basel) 12 (9), 1938. https://doi.org/10.3390/polym12091938.

Aziz, S.B., Brza, M.A., Nofal, M.M., Abdulwahid, R.T., Hussen, S.A., Hussein, A.M., Karim, W.O., 2020c. A Comprehensive Review on Optical Properties of Polymer Electrolytes and Composites. Materials 13, 3675. https://doi.org/10.3390/ma13173675.

Aziz, S.B., Nofal, M.M., Ghareeb, H.O., Dannoun, E.M.A., Hussen, S.A., Hadi, J.M., Ahmed, K.K., Hussein, A.M., 2021a. Characteristics of Poly (vinyl Alcohol)(PVA) Based Composites Integrated with Green Synthesized Al3+-Metal Complex: Structural, Optical, and Localized Density of State Analysis. Polymers 13 (8), 1316. https://doi.org/10.3390/polym13081316.

Aziz, S.B., Asnawi, A.S.F.M., Kadir, M.F.Z., Alshehri, S.M., Ahamad, T., Yusof, Y.M., Hadi, J.M., 2021b. Structural, Electrical and Electrochemical Properties of Glycerolized Biopolymers Based on Chitosan (CS): Methylcellulose (MC) for Energy Storage Application. Polymers (Basel) 13, 1183. https://doi.org/10.3390/polym13081183.

Banerjee, M., Jain, A., Mukherjee, G.S., 2019. Microstructural and optical properties of polyvinyl alcohol/manganese chloride composite film. Polym. Compos. 40, E765–E775. https://doi.org/10.1002/pc.25017.

Ben Nasr, T., Maghraoui-Meherzi, H., Ben Abdallah, H., Bennaceur, R., 2013. First principles calculations of electronic and optical properties of Ag2S. Solid State Sci. 26, 65–71. https://doi.org/10.1016/j.solidstatesciences.2013.09.017.

Bhargav, P.B., Mohan, V.M., Sharma, A.K., Rao, V.V.R.N., 2007. Structural, electrical and optical characterization of pure and doped poly (vinyl alcohol) (PVA) polymer electrolyte films. Int. J. Polym. Mater. Polym. Biomater. 56, 579–591. https://doi.org/10.1080/00914030600972790.

Brza, M.A., Aziz, S.B., Anuar, H., Al Hazza, M.H.F., 2019. From green remediation to polymer hybrid fabrication with improved optical band gaps. Int. J. Mol. Sci. 20 (16), 3910. https://doi.org/10.3390/ijms20163910.

Brza, M.A., Aziz, S.B., Anuar, H., Ali, F., Dannoun, E.M.A., Mohammed, S.J., Abdulwahid, R.T., Al-Zangana, S., 2020. Tea from the drinking to the synthesis of metal complexes and fabrication of PVA based polymer composites with controlled optical band gap. Sci. Rep. 10, 1–17. https://doi.org/10.1038/s41598-020-75138-x.

Brza, M.A., Aziz, S.B., Anuar, H., Ali, F., Abdulwahid, R.T., Hadi, J.M., 2021a. Electrochemical Impedance Spectroscopy as a Novel Approach to Investigate the Influence of Metal Complexes on Electrical Properties of Poly(vinyl alcohol) (PVA) Composites. Int. J. Electrochem. Sci. 16. https://doi.org/10.20964/2021.05.22.

Brza, M.A., Aziz, S.B., Anuar, H., Alshehri, S.M., Ali, F., Ahamad, T., Hadi, J.M., 2021b. Characteristics of a Plasticized PVA-Based Polymer Electrolyte Membrane and H+ Conductor for an Electrical Double-Layer Capacitor: Structural, Morphological,

and Ion Transport Properties. Membranes 11 (4), 296. https://doi.org/10.3390/membranes11040296.

Caglar, M., Zor, M., Ilican, S., Caglar, Y., 2006. Effect of indium incorporation on the optical properties of spray pyrolyzed Cd0.22Zn0.78S thin films. Czechoslov. J. Phys. 56, 277–287. https://doi.org/10.1007/s10582-006-0088-4.

Campoy-Quiles, M., Müller, C., Garriga, M., Wang, E., Inganäs, O., Alonso, M.I., 2014. On the complex refractive index of polymer: Fullerene photovoltaic blends. Thin Solid Films 571, 371–376. https://doi.org/10.1016/j.tsf.2014.02.096.

Cheddadi, S., Boubendira, K., Meradji, H., Ghemid, S., Hassan, F.E. H., Lakel, S., Khenata, R., 2017. First-principle calculations of structural, electronic, optical, elastic and thermal properties of MgXAs 2 (X = Si, Ge) compounds. Pramana – J. Phys. 89, 1–10. https://doi.org/10.1007/s12043-017-1486-9.

Diab, M.A., El-Sonbati, A.Z., Morgan, S.M., El-Mogazy, M.A., 2018. Polymer complexes. LXXI. Spectroscopic studies, thermal properties, DNA binding and antimicrobial activity of polymer complexes. Appl. Organomet. Chem. 32 (8), e4378. https://doi.org/10.1002/aoc.v32.810.1002/aoc.4378.

Dianu, M.L., Kriza, A., Stanica, N., Musuc, A.M., 2010. Transition metal M(II) complexes with isonicotinic acid 2-(9-anthryl-methylene)-hydrazide. J. Serbian Chem. Soc. 75, 1515–1531. https://doi.org/10.2298/JSC091113121D.

Edukondalu, A., Kavitha, B., Rahman, S., Gupta, A., Kumar, K.S., 2015. Optical properties of amorphous Na2O-WO3-B2O3 thin films deposited by electron beam evaporation. Optik (Stuttg) 126, 2163–2166. https://doi.org/10.1016/j.ijleo.2015.05.090.

El-Ghamaz, N.A., El-Sonbati, A.Z., Morgan, S.M., 2012. Optical properties of some synthesized azo thin films. J. Mol. Struct. 1027, 92–98. https://doi.org/10.1016/j.molstruc.2012.06.004.

El-Ghamaz, N.A., Diab, M.A., El-Sonbati, A.Z., Morgan, S.M., Salem, O.L., 2017. Polymer complexes. LXVII: Electrical conductivity and thermal properties of polymer complexes of quinoline azo dye. Chem. Pap. 71, 2417–2433. https://doi.org/10.1007/s11696-017-0236-2.

El-Ghamaz, N.A., El-Sonbati, A.Z., El-Mogazy, M.A., 2017. Effect of γ-radiation on the structural and optical properties of poly(3-allyl-5-[(4-nitrophenyl)diazenyl]-2-thioxothiazolidine-4-one) thin films. J. Mol. Liq. 248, 556–563. https://doi.org/10.1016/j.molliq.2017.10.088.

Elimat, Z.M., Zihlif, A.M., Avella, M., 2008. Thermal and optical properties of poly(methyl methacrylate)/calcium carbonate nanocomposite. J. Exp. Nanosci. 3, 259–269. https://doi.org/10.1080/17458080802603715.

El-Sonbati, A.Z., Diab, M.A., Morgan, S.M., Eldesoky, A.M., Balboula, M.Z., 2018. Polymer complexes. LXIX. Some divalent metal(II) polymer complexes of potentially bidentate monomer N-[4-(5-methyl-isoxazol-3-ylsulfamoyl)-phenyl]-acrylamide: Synthesis, spectroscopic characterization, thermal properties, antimicrobial agents and DNA studies. Appl. Organomet. Chem. 32, 1–23. https://doi.org/10.1002/aoc.4207.

El-Sonbati, A.Z., Diab, M.A., Eldesoky, A.M., Morgan, S.M., Salem, O.L., 2019. Polymer complexes. LXXVI. Synthesis, characterization, CT-DNA binding, molecular docking and thermal studies of sulfoxine polymer complexes. Appl. Organomet. Chem. 33, 1–22. https://doi.org/10.1002/aoc.4839.

Fahmy, A., Agudo Jácome, L., Schönhals, A., 2020. Effect of Silver Nanoparticles on the Dielectric Properties and the Homogeneity of Plasma Poly(acrylic acid) Thin Films. J. Phys. Chem. C 124 (41), 22817–22826. https://doi.org/10.1021/acs.jpcc.0c06712.

Fahmy, A., Mohamed, T.A., Abu-Saied, M., Helaly, H., El-Dossoki, F., 2020. Structure/property relationship of polyvinyl alcohol/dimethoxydimethylsilane composite membrane: Experimental and theoretical studies. Spectrochim. Acta - Part A Mol. Biomol. Spectrosc. 228, 117810. https://doi.org/10.1016/j.saa.2019.117810.

Fahmy, A., Abou-Saied, M., Helaly, H., El-Dessoki, F., Mohamed, T. A., 2021. Novel PVA/Methoxytrimethylsilane elastic composite

membranes: preparation, characterization and DFT computation. J. Mol. Struct. 1235, 130173. https://doi.org/10.1016/j.molstruc.2021.130173.

Ghanipour, M., Dorranian, D., 2013. Effect of Ag-Nanoparticles Doped in Polyvinyl Alcohol on the Structural and Optical Properties of PVA Films. J. Nanomater. 2013, 1–10. https://doi.org/10.1155/2013/897043.

Hadi, J.M., Aziz, S.B., Mustafa, M.S., Brza, M.A., Hamsan, M.H., Kadir, M.F.Z., Ghareeb, H.O., Hussein, S.A., 2020. Electrochemical impedance study of proton conducting polymer electrolytes based on PVC doped with thiocyanate and plasticized with glycerol. Int. J. Electrochem. Sci. 15, 4671–4683. https://doi.org/10.20964/2020.05.34.

Hadi, J.M., Aziz, S.B., Saeed, S.R., Brza, M.A., Abdulwahid, R.T., Hamsan, M.H., Abdullah, R.M., Kadir, M.F.Z., Muzakir, S.K., 2020. Investigation of ion transport parameters and electrochemical performance of plasticized biocompatible chitosan-based proton conducting polymer composite electrolytes. Membranes (Basel) 10, 1–27. https://doi.org/10.3390/membranes10110363.

Hadi, J.M., Aziz, S.B., Nofal, M.M., Hussen, S.A., Hamsan, M.H., Brza, M.A., Abdulwahid, R.T., Kadir, M.F.Z., Woo, H.J., 2020. Electrical, dielectric property and electrochemical performances of plasticized silver ion-conducting chitosan-based polymer nanocomposites. Membranes (Basel) 10, 1–22. https://doi.org/10.3390/membranes10070151.

Hazari, P.P., Pandey, A.K., Chaturvedi, S., Tiwari, A.K., Chandna, S., Dwarakanath, B.S., Mishra, A.K., 2012. Synthesis of Oxovanadium(IV) Schiff base Complexes derived from C-substituted Diamines and Pyridoxal-5-Phosphate as Antitumor Agents. Chem. Biol. Drug Des. 79, 223–234. https://doi.org/10.1111/j.1747-0285.2011.01265.x.

Hecht, E., 2002. Optics, fourth edition, Ch. 3, pp. 74, Adison Wesley.

Herrmann, W.A., Kohlpaintner, C.W., 1993. Water-Soluble Ligands, Metal Complexes, and Catalysts: Synergism of Homogeneous and Heterogeneous Catalysis. Angew. Chemie Int. Ed. English 32 (11), 1524–1544. https://doi.org/10.1002/anie.199315241.

Hussein, A.M., Dannoun, E.M.A., Aziz, S.B., Brza, M.A., Abdulwahid, R.T., Hussen, S.A., Rostam, S., Mustafa, D.M.T., Muhammad, D.S., 2020. Steps Toward the Band Gap Identification in Polystyrene Based Solid Polymer Nanocomposites Integrated with Tin Titanate Nanoparticles. Polymers 12, 2320. https://doi.org/10.3390/polym12102320.

Hussen, S.A., 2020. Structural and optical characterization of pure and SnZrO3 doped PS based polymer nanocomposite. Mater. Res. Express. 7, 105302.

Islam, S.I., Das, S.B., Chakrabarty, S., Hazra, S., Pandey, A., Patra, A., 2016. Synthesis, Characterization, and Biological Activity of Nickel (II) and Palladium (II) Complex with Pyrrolidine Dithiocarbamate (PDTC). Adv. Chem. 2016, 1–6. https://doi.org/10.1155/2016/4676524.

Jiang, M., Li, J., Huo, Y.Q., Xi, Y., Yan, J.F., Zhang, F.X., 2011. Synthesis, thermoanalysis, and thermal kinetic thermogravimetric analysis of transition metal Co(II), Ni(II), Cu(II), and Zn(II) complexes with 2-(2-Hydroxyphenyl)benzimidazole (HL). J. Chem. Eng. Data 56, 1185–1190. https://doi.org/10.1021/je101107w.

Kavitha, N., Anantha Lakshmi, P.V., 2017. Synthesis, characterization and thermogravimetric analysis of Co(II), Ni(II), Cu(II) and Zn(II) complexes supported by ONNO tetradentate Schiff base ligand derived from hydrazino benzoxazine. J. Saudi Chem. Soc. 21, S457–S466. https://doi.org/10.1016/j.jscs.2015.01.003.

Kershaw, S.V., Susha, A.S., Rogach, A.L., 2013. Narrow bandgap colloidal metal chalcogenide quantum dots: Synthetic methods, heterostructures, assemblies, electronic and infrared optical properties. Chem. Soc. Rev. 42, 3033–3087. https://doi.org/10.1039/c2cs35331h.

Kesavan, K., Mathew, C.M., Rajendran, S., 2014. Lithium ion conduction and ion-polymer interaction in poly(vinyl pyrrolidone) based electrolytes blended with different plasticizers. Chinese

Chem. Lett. 25, 1428–1434. https://doi.org/10.1016/j.cclet.2014.06.005.

Kymakis, E., Amaratunga, G.A.J., 2004. Optical properties of polymer-nanotube composites. Synth. Met. 142, 161–167. https://doi.org/10.1016/j.synthmet.2003.08.011.

Lahneche, Y.D., Boulebd, H., Benslimane, M., Bencharif, M., Belfaitah, A., 2019. Dinuclear Hg(II) complex of new benzimidazole-based Schiff base: one-pot synthesis, crystal structure, spectroscopy, and theoretical investigations. J. Coord. Chem. 72 (18), 3156–3170. https://doi.org/10.1080/00958972.2019.1680833.

Li, L., Wang, W., Liu, H., Liu, X., Song, Q., Ren, S., 2009. First Principles Calculations of Electronic Band Structure and Optical Properties of Cr-Doped ZnO. J. Phys. Chem. C 113, 8460–8464. https://doi.org/10.1021/jp811507r.

Liu, S.-J., Chen, Y., Xu, W.-J., Zhao, Q., Huang, W., 2012. New trends in the optical and electronic applications of polymers containing transition-metal complexes. Macromol. Rapid Commun. 33 (6-7), 461–480. https://doi.org/10.1002/marc.201100775.

Liu, Y., Li, Y., Schanze, K.S., 2002. Photophysics of π-conjugated oligomers and polymers that contain transition metal complexes. J. Photochem. Photobiol. C Photochem. Rev. 3 (1), 1–23. https://doi.org/10.1016/S1389-5567(02)00004-7.

Mahmoudi, H., Bagherzadeh, M., Ataie, S., Kia, R., Heydar Moravej, S., Zare, M., Raithby, P.R., Ferlin, F., Vaccaro, L., 2020. Synthesis and X-ray crystal structure of a Molybdenum(VI) Schiff base complex: Design of a new catalytic system for sustainable olefin epoxidation. Inorg. Chim. Acta 511, 119775. https://doi.org/10.1016/j.ica.2020.119775.

McCormick, B.J., 1968. The Structure and Spectra of Dithiocarbamate Complexes of Oxovanadium(IV). Inorg. Chem. 7 (10), 1965–1970. https://doi.org/10.1021/ic50068a002.

Menezes, D.C., Vieira, F.T., de Lima, G.M., Porto, A.O., Cortés, M.E., Ardisson, J.D., Albrecht-Schmitt, T.E., 2005. Tin(IV) complexes of pyrrolidinedithiocarbamate: Synthesis, characterisation and antifungal activity. Eur. J. Med. Chem. 40 (12), 1277–1282. https://doi.org/10.1016/j.ejmech.2005.07.008.

Mohan, V.M., Bhargav, P.B., Raja, V., Sharma, A.K., Rao, V.V.R.N., 2007. Optical and electrical properties of pure and doped PEO polymer electrolyte films. Soft Mater 5, 33–46. https://doi.org/10.1080/15394450701405291.

Mohan, V.M., Raja, V., Bhargav, P.B., Sharma, A.K., Rao, V.V.R.N., 2007. Structural, electrical and optical properties of pure and NaLaF4 doped PEO polymer electrolyte films. J. Polym. Res. 14, 283–290. https://doi.org/10.1007/s10965-007-9108-8.

Morgan, S.M., Diab, M.A., El-Sonbati, A.Z., 2018. Synthesis, spectroscopic, thermal properties, Calf thymus DNA binding and quantum chemical studies of M(II) complexes. Appl. Organomet. Chem. 32, 1–25. https://doi.org/10.1002/aoc.4281.

Morgan, S.M., Diab, M.A., El-Sonbati, A.Z., 2018. Synthesis, molecular geometry, spectroscopic studies and thermal properties of Co(II) complexes. Appl. Organomet. Chem. 32 (4), e4305. https://doi.org/10.1002/aoc.v32.410.1002/aoc.4305.

Morsali, A., Masoomi, M.Y., 2009. Structures and properties of mercury(II) coordination polymers. Coord. Chem. Rev. 253 (13-14), 1882–1905. https://doi.org/10.1016/j.ccr.2009.02.018.

Muhammad, F.F., Sulaiman, K., 2011. Photovoltaic performance of organic solar cells based on DH6T/PCBM thin film active layers. Thin Solid Films 519, 5230–5233. https://doi.org/10.1016/j.tsf.2011.01.165.

Muhammad, F.F., Sulaiman, K., 2011. Utilizing a simple and reliable method to investigate the optical functions of small molecular organic films - Alq3 and Gaq3 as examples. Meas. J. Int. Meas. Confed. 44, 1468–1474. https://doi.org/10.1016/j.measurement.2011.05.017.

Muhammed, D.S., Brza, M.A., Nofal, M.M., Aziz, S.B., Hussen, S.A., Abdulwahid, R.T., 2020. Optical dielectric loss as a novel approach to specify the types of electron transition: XRD and UV-vis as a non-destructive techniques for structural and optical characteriza-

tion of peo based nanocomposites. Materials (Basel) 13, 1–15. https://doi.org/10.3390/ma13132979.

Nimrodh Ananth, A., Umapathy, S., Sophia, J., Mathavan, T., Mangalaraj, D., 2011. On the optical and thermal properties of in situ/ex situ reduced Ag NP's/PVA composites and its role as a simple SPR-based protein sensor. Appl. Nanosci. 1 (2), 87–96. https://doi.org/10.1007/s13204-011-0010-7.

Nofal, M.M., Aziz, S.B., Hadi, J.M., Abdulwahid, R.T., Dannoun, E.M.A., Marif, A.S., Al-Zangana, S., Zafar, Q., Brza, M.A., Kadir, M.F.Z., 2020. Synthesis of porous proton ion conducting solid polymer blend electrolytes based on PVA: CS polymers: Structural, morphological and electrochemical properties. Materials (Basel) 13, 1–21. https://doi.org/10.3390/ma13214890.

Sari, N., Gürkan, P., 2004. Some novel amino acid-schiff bases and their complexes synthesis, characterization, solid state conductivity behaviors and potentiometric studies. Zeitschrift fur Naturforsch. - Sect B J. Chem. Sci. 59, 692–698. https://doi.org/10.1515/znb-2004-0610.

Sarma, B., Das, D.K., 2013. Synthesis, spectroscopy, thermal analysis, electrochemistry and superoxide scavenging activity of a new bimetallic copper(II) complex. J. Chem. 2013, 1–6. https://doi.org/10.1155/2013/349580.

Sekerci, M., Yakuphanoglu, F., 2004. Thermal analysis study of some transition metal complexes by TG and DSC methods. J. Therm. Anal. Calorim. 75, 189–195. https://doi.org/10.1023/B:JTAN.0000017341.20105.22.

Seto, R., Kojima, T., Hosokawa, K., Koyama, Y., Konishi, G.I., Takata, T., 2010. Synthesis and property of 9,9′-spirobifluorene-containing aromatic polyesters as optical polymers with high refractive index and low birefringence. Polymer (Guildf) 51, 4744–4749. https://doi.org/10.1016/j.polymer.2010.08.032.

Shi, W., Fang, C., Yin, X., Pan, Q., Sun, X., Qintian, Gu., Yu, J., 1999. Refractive index dispersion measurement on nonlinear optical polymer using V-prism refractometer. Opt. Lasers Eng. 32, 41–47. https://doi.org/10.1016/S0143-8166(99)00047-0.

Shi, S., Yu, S., Quan, L., Mansoor, M., Chen, Z., Hu, H., Liu, D., Liang, Y., Liang, F., 2020. Synthesis and antitumor activities of transition metal complexes of a bis-Schiff base of 2-hydroxy-1-naphthalenecarboxaldehyde. J. Inorg. Biochem. 210, 111173. https://doi.org/10.1016/j.jinorgbio.2020.111173.

Soliman, T.S., Vshivkov, S.A., Elkalashy, S.I., 2020. Structural, linear and nonlinear optical properties of Ni nanoparticles – Polyvinyl alcohol nanocomposite films for optoelectronic applications. Opt. Mater. (Amst) 107, 110037. https://doi.org/10.1016/j.optmat.2020.110037.

Steyl, J.D.T., 2009. Kinetic modelling of chemical processes in acid solution at t ≤ 200°C. (i) thermodynamics and speciation in H2SO4-Metal (II) SO4-H2O system. Hydrometall. Conf., 401–444

Stoyanov, H.Y., Stefanov, I.L., Tsutsumanova, G.G., Russev, S.C., Hadjichristov, G.B., 2012. Depth-profiled characterization of complex refractive index of ion implanted optically transparent polymers using multilayer calculations and reflectance data. Vacuum 86, 1822–1827. https://doi.org/10.1016/j.vacuum.2012.04.030.

Taib, M.F.M., Yaakob, M.K., Hassan, O.H., Yahya, M.Z.A., 2012. First principles calculation on elastic, electronic and optical properties of new cubic (Pm3m) pb-free perovskite oxide of SnZrO3. In: ISBEIA 2012 - IEEE Symp. Business, Eng. Ind. Appl., pp. 13–17. https://doi.org/10.1109/ISBEIA.2012.6422855.

Tao, P., Li, Y., Rungta, A., Viswanath, A., Gao, J., Benicewicz, B.C., Siegel, R.W., Schadler, L.S., 2011. TiO2 nanocomposites with high refractive index and transparency. J. Mater. Chem. 21, 18623–18629. https://doi.org/10.1039/c1jm13093e.

Thutupalli, G.K.M., Tomlin, S.G., 1976. The optical properties of thin films of cadmium and zinc selenides and tellurides. J. Phys. D. Appl. Phys. 9, 1639–1646. https://doi.org/10.1088/0022-3727/9/11/010.

Wang, Z., Lu, Z., Mahoney, C., Yan, J., Ferebee, R., Luo, D., Matyjaszewski, K., Bockstaller, M.R., 2017. Transparent and High Refractive Index Thermoplastic Polymer Glasses Using Evapora-

tive Ligand Exchange of Hybrid Particle Fillers. ACS Appl. Mater. Interfaces 9, 7515–7522. https://doi.org/10.1021/acsami.6b12666.

Wang, Y., Ye, W., Yang, X., Rezaee, E., Shan, H., Yang, S., Cai, S., Pan, J.-H., Xu, J., Xu, Z.-X., 2020. Hole transport layers based on metal Schiff base complexes in perovskite solar cells. Synth. Met. 259, 116248. https://doi.org/10.1016/j.synthmet.2019.116248.

Xu, H., Chen, R., Sun, Q., Lai, W., Su, Q., Huang, W., Liu, X., 2014. Recent progress in metal-organic complexes for optoelectronic applications. Chem. Soc. Rev. 43, 3259–3302. https://doi.org/10.1039/c3cs60449g.

Xu, Y., Shi, Y., Lei, F., Dai, L., 2020. A novel and green cellulose-based Schiff base-Cu (II) complex and its excellent antibacterial activity. Carbohydr. Polym. 230, 115671. https://doi.org/10.1016/j.carbpol.2019.115671.

Yosef, M., Fahmy, A., Hotaby, W.E., Hassan, A.M., Khalil, A.S.G., Anis, B., 2020. High performance graphene-based PVF foam for lead removal from water. J. Mater. Res. Technol. 9 (5), 11861–11875. https://doi.org/10.1016/j.jmrt.2020.08.011.

Zhang, H., Wu, J.S., Peng, F., 2008. Potent anticancer activity of pyrrolidine dithiocarbamate-copper complex against cisplatin-resistant neuroblastoma cells. Anticancer Drugs 19, 125–132. https://doi.org/10.1097/CAD.0b013e3282f2bdff.

Zhao, X.Y., Wang, Y.H., Zhang, M., Zhao, N., Gong, S., Chen, Q., 2011. First-principles calculations of the structural, electronic and optical properties of BaZrxTi1-xO3 (x = 0, 0.25, 0.5, 0.75). Chinese Phys. Lett. 28, 3–6. https://doi.org/10.1088/0256-307X/28/6/067101.

Zulkifli, A.M., Aqilah Mat Said, N.I., Aziz, S.B., Ali Dannoun, E.M., Hisham, S., Shah, S., Bakar, A.A., Zainal, Z.H., Tajuddin, H.A., Hadi, J.M., Brza, M.A., Saeed, S.R., Amin, P.O., 2020. Characteristics of Dye-Sensitized Solar Cell Assembled from Modified Chitosan-Based Gel Polymer Electrolytes Incorporated with Potassium Iodide. Molecules 25. https://doi.org/10.3390/molecules25184115.